arXiv:1410.2754v3 [hep-ph] 14 Oct 2014

Pseudoscalar meson photoproduction on nucleon target

G.H. Arakelyan[1], C. Merino[2] and Yu.M. Shabelski[3]

[1]A.I.Alikhanyan Scientific Laboratory
Yerevan Physics Institute
Yerevan 0036, Armenia
e-mail: argev@mail.yerphi.am

[2]Departamento de Física de Partículas, Facultade de Física
and Instituto Galego de Física de Altas Enerxías (IGFAE)
Universidade de Santiago de Compostela
15782 Santiago de Compostela
Galiza, Spain
e-mail: merino@fpaxp1.usc.es

[3]Petersburg Nuclear Physics Institute
NCR Kurchatov Institute
Gatchina, St.Petersburg 188350, Russia
e-mail: shabelsk@thd.pnpi.spb.ru

Abstract

We consider the photoproduction of secondary mesons in the framework of the Quark-Gluon String model. At relatively low energies, not only cylindrical, but also planar diagrams have to be accounted for. To estimate the significant contribution of planar diagrams in γp collisions at rather low energies, we have used the expression obtained from the corresponding phenomenological expression for πp collisions. The results obtained by the model are compared to the existing SLAC experimental data. The model predictions for light meson production at HERMES energies are also presented.

1 Introduction

The physical photon state is approximately represented by the superposition of a bare photon and of virtual hadronic states having the same quantum numbers as the photon. The bare photon may interact in direct processes. This direct contribution is determined by the lowest order in perturbative QED. The interactions of the hadronic components of the photon (resolved photons) at high enough energies are described within the framework of theoretical models based on Reggeon and Pomeron exchanges, like the Dual-Parton model (DPM), see [1] for a review, and the Quark-Gluon String model (QGSM) [2, 3].

The QGSM is based on the Dual Topological Unitarization (DTU) and on the large 1/N expansion of non-perturbative QCD, and it has been very successful in describing many features of the inclusive hadroproduction of secondaries, both at high [3]-[6], and at comparatively low [7, 8, 9] energies.

In the case of photoproduction processes, QGSM was used in [10, 11] at energies higher then 100 GeV. At these high energies the accounting for only pomeron (cylindrical) diagrams leads to a reasonable agreement. However, at low energies one can nott neglect the contribution of planar diagrams [7, 8, 9]. The inclusion of palnar diagrams into the analysis of pp scattering should result in the better description of a wider range of experimental data.

Most interesting it is the comparison of secondary production by photon and hadron beams in their fragmentation regions. The photoproduction ($Q^2 = 0$) points are the boundary ($Q^2 \to 0$) for the electroproduction processes [12].

In the present paper we apply QGSM to the low energy photoproduction of pions and kaons by taking into accaount, contrary to [10, 11], both cylindrical and planar diagrams. We describe the SLAC experimental data [13, 14] on inclusive x_F spectra integrated over p_T. The predictions for forthcoming quasireal photoproduction data at HERMES and JLAB energies are also presented.

2 Inclusive spectra of secondary hadrons in photoproduction processes

Let us now consider the photoproduction processes in the QGSM. The resolved photon can be consider as

$$|\gamma >= \frac{1}{6}(4|\overline{u}u > +|\overline{d}d > +|\overline{s}s >) \, , \tag{1}$$

in agreement with standard Vector Dominance Model (VDM) expansion [15], and so the quarks in Eq. 1 can be considered as the valence quarks of a meson. This resolved photon state also has sea quarks and gluons, as usual hadrons.

We can calculate the photoproduction cross section like for a meson-nucleon process* by summing, according to Eq. 1, the contribution of $q\bar{q}$ pair collisions with target nucleon, and by taking into account the corresponding coefficients.

At low energies, the inclusive cross section in QGSM consists of two terms, described by two different types of diagrams: cylindrical and planar.

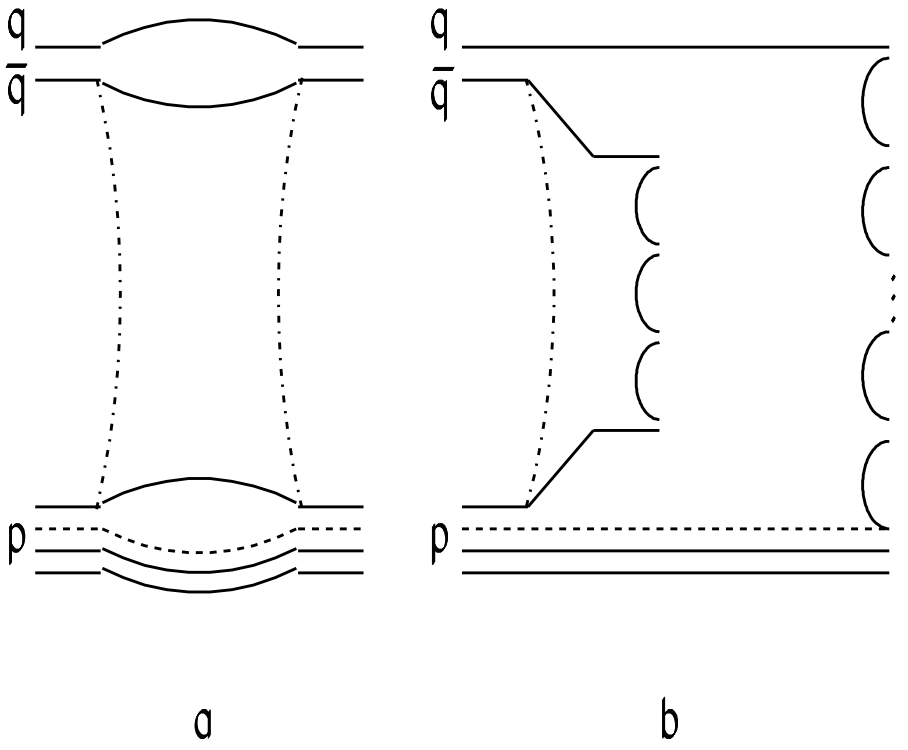

Figure 1: (a) Cylindrical diagram corresponding to the one-Pomeron exchange contribution to elastic $q\bar{q}$ scattering, and (b) the cut of this diagram which determines the contribution to the inelastic $q\bar{q}$ cross section. Quarks are shown by solid curves, while SJ is shown by dashed curves.

$$\frac{dn}{dy} = \frac{1}{\sigma_{inel}}\frac{d\sigma}{dy} = \frac{dn^{cyl}}{dy} + \frac{dn^{pl}}{dy} \tag{2}$$

In QGSM high energy interactions are considered as takin place via the exchange of one or several Pomerons, and all elastic and inelastic processes result from cutting through or between pomerons [18] (see Fig.1). Each Pomeron corresponds to a cylindrical diagram (see Fig. 1a), and thus, when cutting a Pomeron, two showers of secondaries are produced, as it is shown in Fig. 1b.

*The absolute values of secondary photoproducton cross section are α_{em} times those of meson-nucleon cross section, while the corresponding multiplicities of secondaries $\frac{dn}{dy}$ are of the same order.

For γp interaction, that following Eq. 1 is similar to πp collisions, the inclusive spectrum of a secondary hadron h produced from a $q\overline{q}$ pair has the form [5, 6]:

$$\frac{dn^{cyl}}{dy} = \frac{x_E}{\sigma_{inel}}\frac{d\sigma^{cyl}}{dx_F} = \sum_{n=1}^{\infty} w_n \phi_n^h(x) \ , \tag{3}$$

where $x_F = 2p_{\parallel}/\sqrt{s}$ is the Feynman variable, $x_E = 2E/\sqrt{s}$, the functions $\phi_n^h(x)$ determine the contribution of diagrams with n cut Pomerons, and w_n is the relative weight of these diagrams. Thus,

$$\begin{aligned} \phi^h_{q\overline{q}p}(x) &= f^h_{\overline{q}}(x_+,n)\cdot f^h_q(x_-,n) + f^h_q(x_+,n)\cdot f^h_{qq}(x_-,n) \\ &+ 2(n-1) f^h_{sea}(x_+,n)\cdot f^h_{sea}(x_-,n) \ , \qquad (4) \\ x_\pm &= \frac{1}{2}\left[\sqrt{4m_T^2/s + x^2} \ \pm x\right], \qquad (5) \end{aligned}$$

where f_{qq}, f_q, and f_{sea} correspond to the contributions of diquarks, valence quarks and sea quarks, respectively. These functions f_{qq}, f_q, and f_{sea} are determined by the convolution of the diquark and quark distribution functions, $u(x,n)$, with the fragmentation functions, $G^h(z)$, to hadron h, e.g.

$$f_i^h(x_+,n) = \int_{x_+}^{1} u_i(x_1,n) G_i^h(x_+/x_1) dx_1 \ , \tag{6}$$

where $i = q, \overline{q}, qq$-diquarks, and sea quarks.

The fragmentatiion functions $G_i^{\pi}(z)$ have the same value, a^{π} at $z \to 0$ for all i. Similarly, $G_i^K(z)$ have also the same value, a^K at $z \to 0$ for all i. The numerical values of these parameters are [16]:

$$a^{\pi} = 0.68, \ a^K = 0.26 \ . \tag{7}$$

The diquark and quark distribution functions, which are normalized to unity, as well as the fragmentation functions, are determined from Regge intercepts [19]. The analytical expressions of these functions for proton are presented in [5, 6]. The distribution functions for quarks and antiquarks in a photon were obtained by using the simplest interpolation of Regge limits at $u_i(x \to 0)$ and $u_i(x \to 1)$, following [5, 6]. In the sum of all cylindrical diagrams we have used the weights given in Eq. 1.

At low energies the contribution of planar diagrams becomes significant. In particular, planar diagrams lead to the difference from $\sigma_{tot}^{\pi^- p}$ (Fig. 2a) to $\sigma_{tot}^{\pi^+ p}$(Fig. 2b) total cross sections.

Since the proton contains two u quarks and one d quark, there are two planar diagrams contributing to $\sigma_{tot}^{\pi^- p}$ (Fig. 2a), and only one contributing to $\sigma_{tot}^{\pi^+ p}$ (Fig. 2b). By neglecting the difference in $u\overline{u}$ and $d\overline{d}$ annihilation, we can consider as equal the

contribution by every planar diagram. If we denote this contribution by each planar digram as $\sigma_{pl}^{\pi p}$, the contribution of diagrams in Fig. 2a to the $\sigma_{tot}^{\pi^- p}$ is $2\sigma_{pl}^{\pi p}$, while the contribution of Fig. 2b to the total $\sigma_{tot}^{\pi^+ p}$ cross section is $\sigma_{pl}^{\pi p}$. Thus,

$$\Delta\sigma(\pi^{\mp} p) = \sigma_{tot}(\pi^- p) - \sigma_{tot}(\pi^+ p) = \sigma_{pl}^{\pi p} \ , \tag{8}$$

the cylindrical contributions cancelling each other off into the difference. One

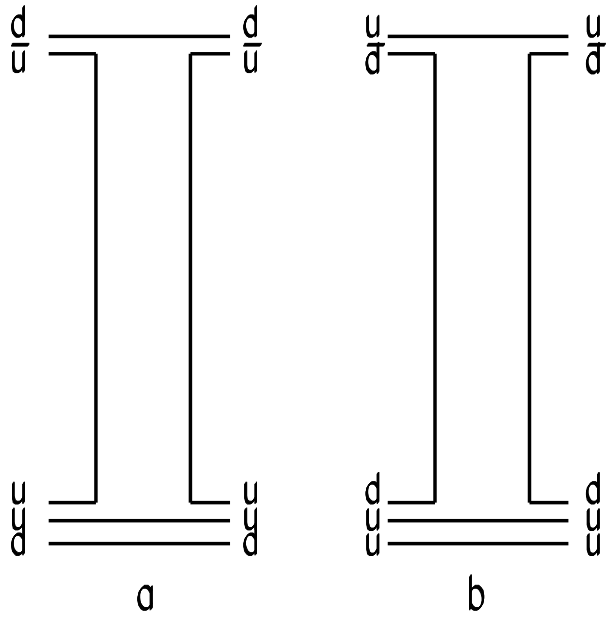

Figure 2: Planar diagrams for the (a) $\pi^- p$ and (b) $\pi^+ p$ elastic scattering amplitudes.

can find $\overline{u}$ quark in the photon with probability $\frac{4}{6}$ (see Eq. 1), and so, simply from comparison of the number of diagrams of figs. 2a and 3a at the same energies, there is a contribution to planar photoproduction cross section from the diagram Fig. 3a (strange quarks do not contribute to planar photoproduction) equal to

$$\frac{\sigma_{pl}^{\gamma p(3a)}}{\sigma_{inel}^{\gamma p}} = \frac{4}{3}\frac{\sigma_{pl}^{\pi p}}{\sigma_{inel}^{\pi p}} \ , \tag{9}$$

and, in a similar way, the contribution to planar photoproduction cross section from the diagram Fig. 3b is

$$\frac{\sigma_{pl}^{\gamma p(3b)}}{\sigma_{inel}^{\gamma p}} = \frac{1}{6}\frac{\sigma_{pl}^{\pi p}}{\sigma_{inel}^{\pi p}} \ , \tag{10}$$

with $\sigma_{tot}^{\gamma p} \cong \sigma_{inel}^{\gamma p}$ in both cases. Thus, the resulting contribution from planar photoprouction coming from diagrams in figs. 3a and 3b to the inclusive cross section is determined by using similar formula to those in [2, 8]:

$$\frac{dn_{pl}^{\gamma p}}{dy} \quad = \quad \frac{\sigma_{pl}^{\gamma p}}{\sigma_{inel}^{\gamma p}}[\frac{4}{3}G_u^h(x_+)G_{ud}^h(x_-) + \frac{1}{6}G_d^h(x_+)G_{uu}^h(x_-)] \tag{11}$$

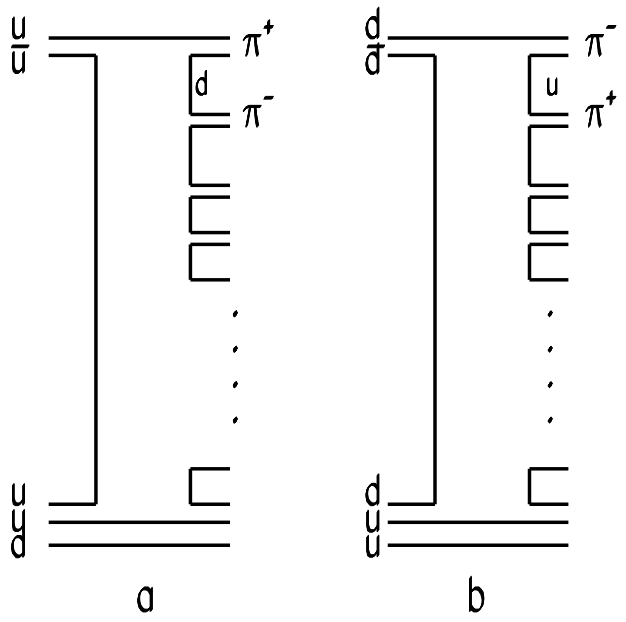

Figure 3: Planar diagrams describing secondary meson M production (a) by u and (b) by d valence quarks from photon.

$$= \frac{\Delta\sigma(\pi^{\mp}p)}{\sigma_{inel}^{\pi p}}[\frac{4}{3}G_u^h(x_+)G_{ud}^h(x_-) + \frac{1}{6}G_d^h(x_+)G_{uu}^h(x_-)] \qquad (12)$$

The parametrisation of experimental data on $\Delta\sigma(\pi^{\mp}p)$ at $\sqrt{s} \geq 5$GeV exists [17]:

$$\Delta\sigma(\pi^{\mp}p) = 2.161(\frac{s}{s_M})^{-0.544}\text{mb} \ , \qquad (13)$$

where $s_M = (\mu + m_p + 2.177)^2$, μ is the pion mass, and m_p is the proton mass. At energies $\sqrt{s} \approx 5GeV$, where the contribution of planar diagrams is not negligible, $\sigma_{inel}^{\pi p} \approx 26$ mb.

For K-mesons photoproduction, the planar diagrams exist only for leading K^+ production, since only the u-quark in the photon can create the planar diagram in the collision with the target proton. On the other hand, the K^--meson can be produced in a planar diagram as a slower nonleading particle.

3 Results of calculations

In this section, we present the results of the QGSM calculation for pseudoscalar meson photoproduction on a proton target. Thus, in Fig. 4 we compare the QGSM

results with the experimental data on π^0 photoproduction obtained by OMEGA collaboration [13]. In this experiment the cross sections were measured at photon energies of 110−135 GeV, 85−110 GeV, and 50−85 GeV. The theoretical curves in Fig. 4 have been calculated at photon energies 120 GeV (dashed line), 100 GeV (full line), and 70GeV (dashed-dotted line). As we can see, the theoretical curves obtained at these three energies practically coincide, in correspondence to the scaling shown by the experimental data. At these energies the contribution of planar diagrams is small, and the present calculations are close to the results by [11], where the only contribution from cylindrical diagrams was taken into account.

In Fig. 5 we present the comparison of QGSM calculations for the x_F dependence of the K^0_S inclusive cross section $F(x_F) = (1/\sigma_{tot})d\sigma/dx_F$, integrated over p^2_T, to the experimental data by [14] at E_γ= 20 GeV. The dashed line corresponds to the contribution from only cylindrical diagrams, while the full curve represents the sum of contributions from both cylindrical and planar diagrams. As we can see, though the contribution of the planar diagrams is not large, its inclusion leads to a better agreement with the experimental data. However, one has to note that the theoretical result is proportional to $(a^K)^2$ (Eq. 7), and the value of this parameter is mainly known from high energy pp collisions, so its accuracy is estimated not to be better then 10% [16].

In Fig. 6 we show the model predictions for the inclusive density of $\pi^\pm$ and $K^\pm$ mesons at the energy of HERMES Collaboration E_γ= 17 GeV. The full curves correspond to the inclusive spectra of π^+ and K^+, while dashed lines represent π^- and K^- meson photoproduction. We show the summed contribution of both cylindrical and planar diagrams.

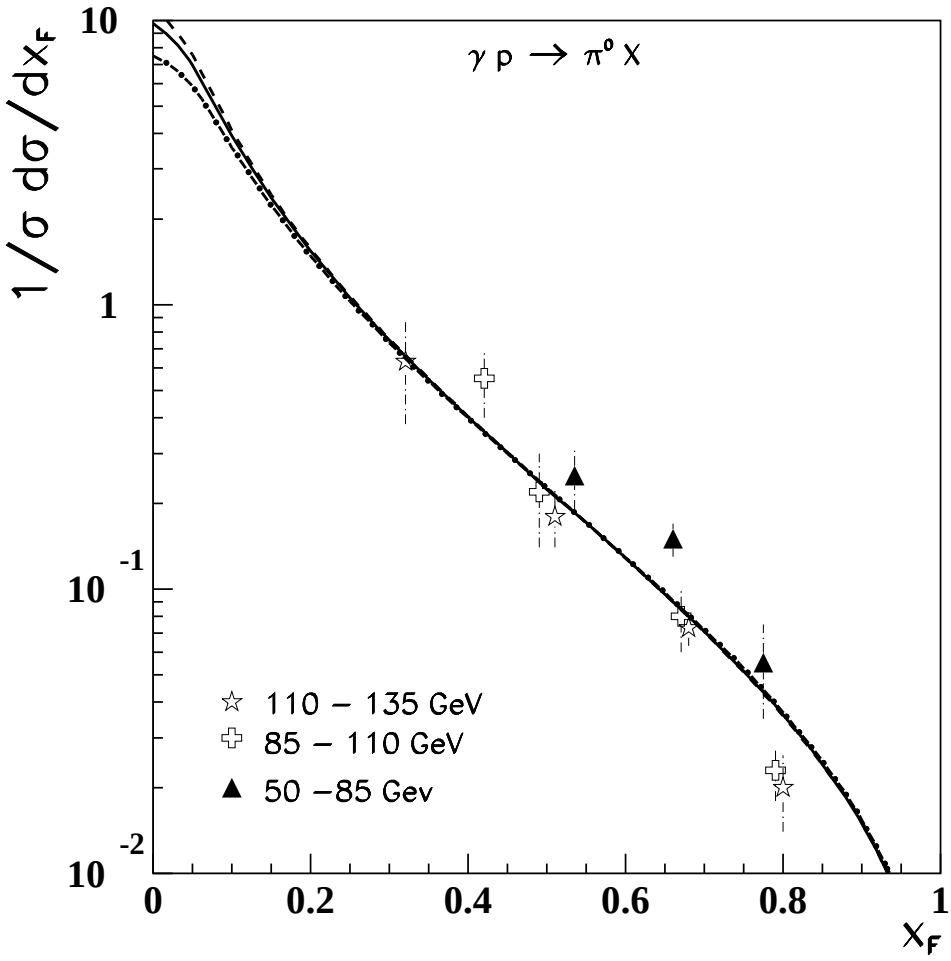

Figure 4: QGSM calculation of the x_F dependence of the π^0 photoproduction cross section integrated over p_T^2, compared to the experimental data [13]. The full line corresponds to calculations at a photon energy of 100 GeV.

The prediction for the ratio of yields of π^+/π^--mesons at E_γ= 17 GeV is shown in Fig. 7 by full line. The cylindrical contribution is shown by dashed line. One can see that the planar diagram contribution changes the ratio by 25% in the forward hemisphere at large x_F.

In Fig. 8 the ratio of yields of K^+/K^--mesons at E_γ= 17 GeV is shown. Only valence u-quark contributes for leading K^+-meson production in planar diagram.

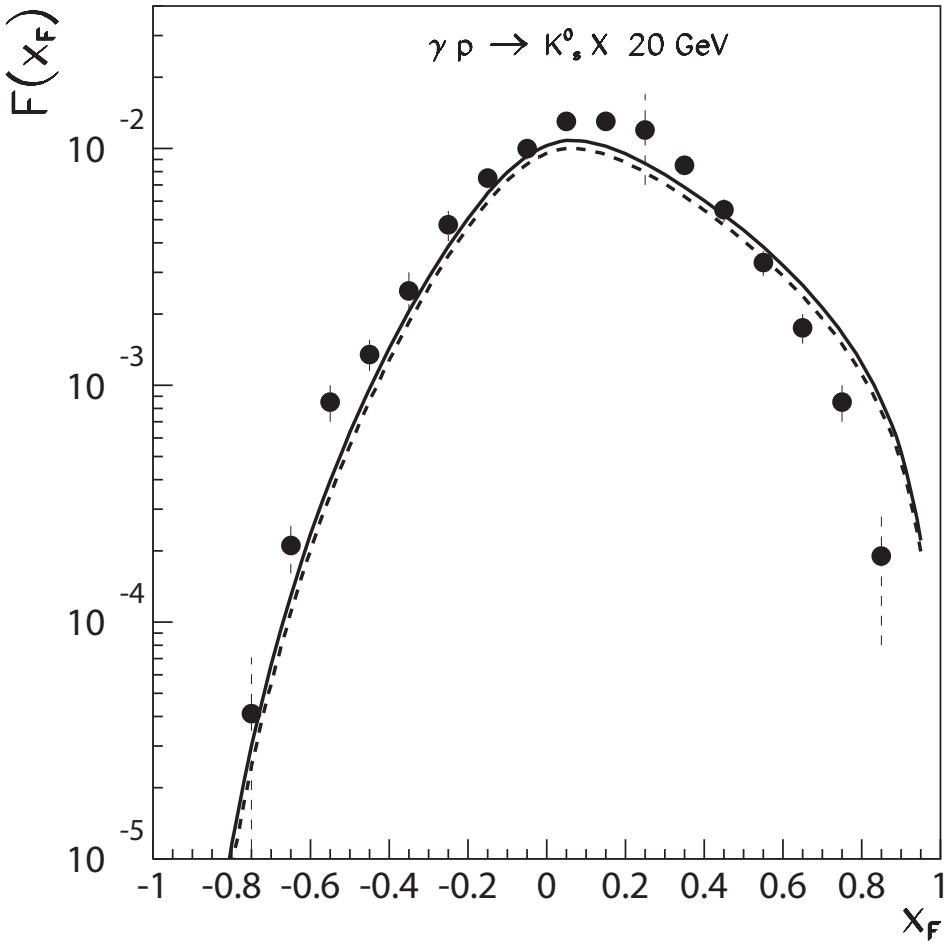

Figure 5: QGSM predictions for the x_F dependence of K^0_S photoproduction cross section integrated over p^2_T, and compared to the experimental data [14]. The full line corresponds to the calculations for a photon energy of 20 GeV, and the dashed line to the corresponding contribution from only cylindrical diagrams.

4 Conclusion

We consider a modified QGSM approach for the description of pseudoscalar (π, K) mesons photoproduction on nucleons at relatively low energies. This approach gives reasonable agreement to the experimental data on the x_F dependence for π^0 cross sections at E_γ=100 GeV, and for K^0_S at E_γ=20 GeV, by taking into account the planar diagrams contribution that becomes significant at low energies. We also present the model predictions for charged pions and kaons cross sections and for the yields ratios at E_γ=17 Gev (Hermes Collaboration energies).

The comparison of the model results with experimental data allows the estimation of the contribution of the planar diagrams to the particle photoproduction processes. Detailed comparison of the theoretical predictions to experimental data at low en-

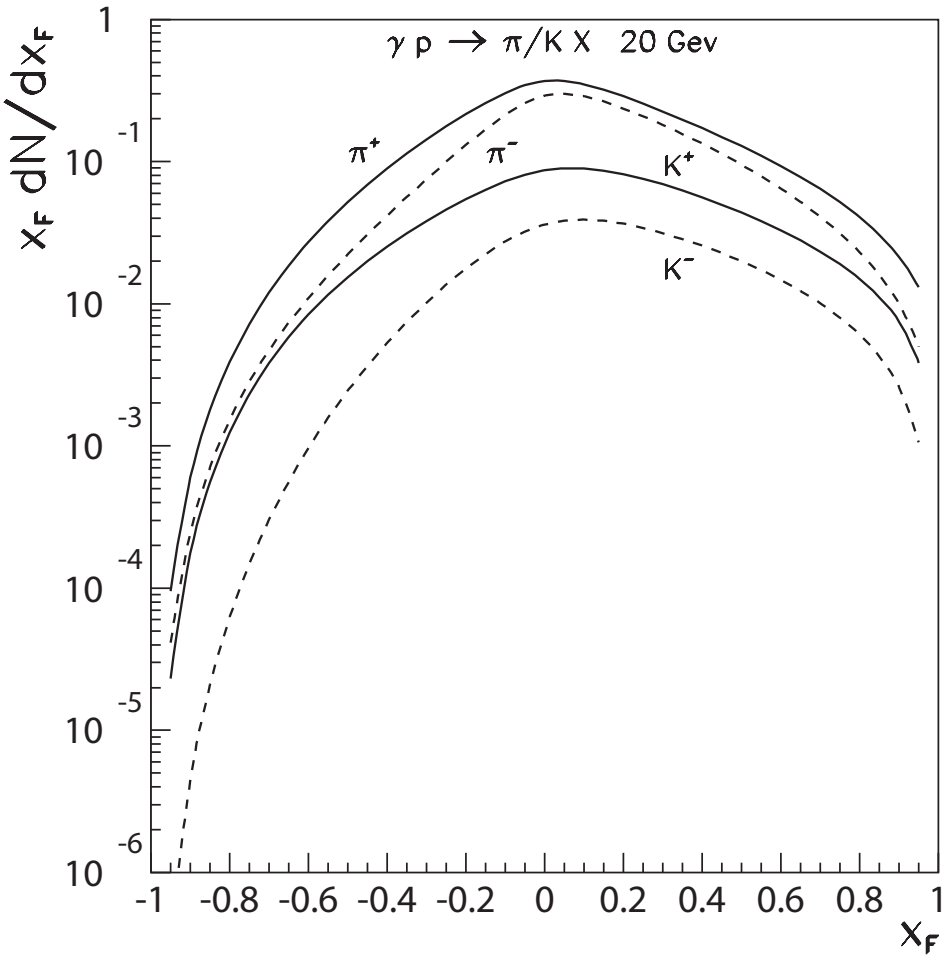

Figure 6: The QGSM prediction for the x_F dependence of the invariant cross section $F(x_F) = 1/\sigma_{tot} d\sigma/dx_F$ integrated over p_T^2 spectra of π^+ (full) and π^- (dashed), upper lines, and of K^+ (full) and K^- (dashed), lower lines, photoproduction at E_γ= 17 GeV.

ergies makes possible to refine the values of the parameters of the model, and, in this way, it improves the reliability of the calculated yields of secondary particles to describe possible future HERMES data of quasireal photoproduction processes.

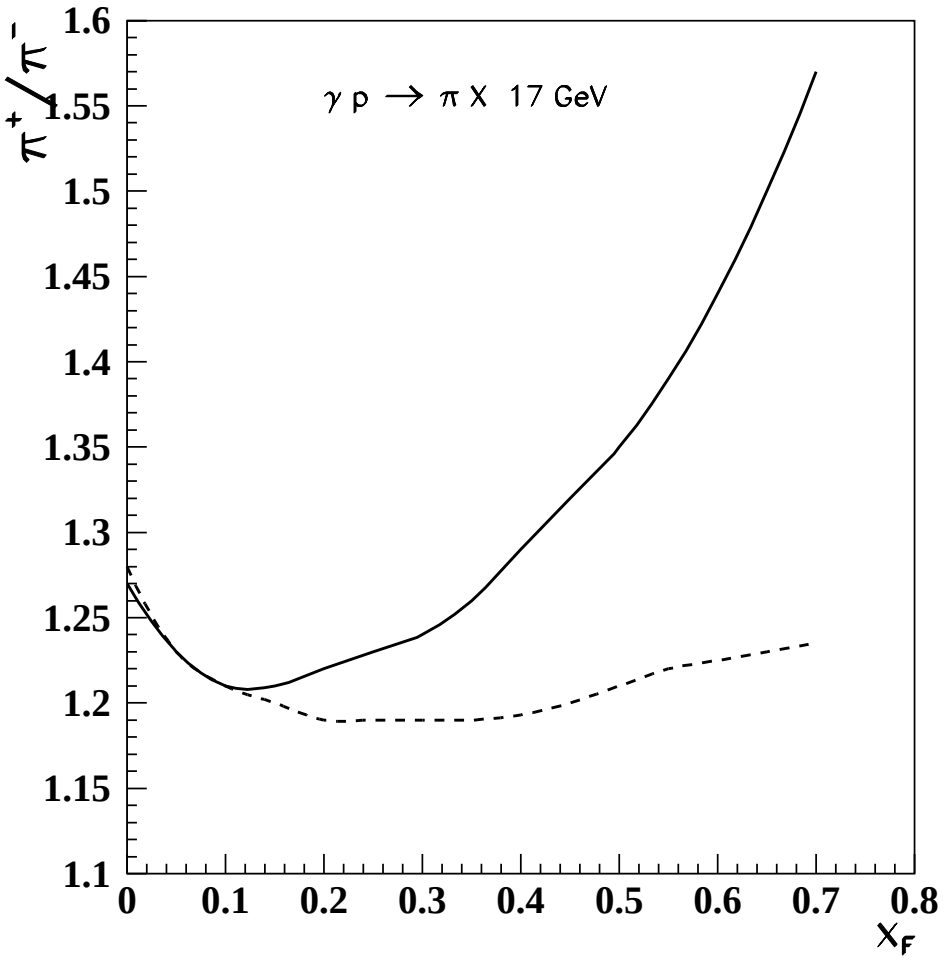

Figure 7: The QGSM prediction for the x_F dependence of the ratio of yields of charged π mesons at E_γ= 17 GeV (full line). The dashed line shows the contribution from only the cylindical diagram.

Acknowledgements

We are grateful to N.Z. Akopov, G.M. Elbakyan, and P.E. Volkovitskii for useful discussions. This paper was supported by the State Committee of Science of Republic of Armenia, Grant-13-1C015, and by Ministerio de Economía y Competitividad of Spain (FPA2011−22776), the Spanish Consolider-Ingenio 2010 Programme CPAN (CSD2007-00042), and Xunta de Galicia, Spain (2011/PC043).

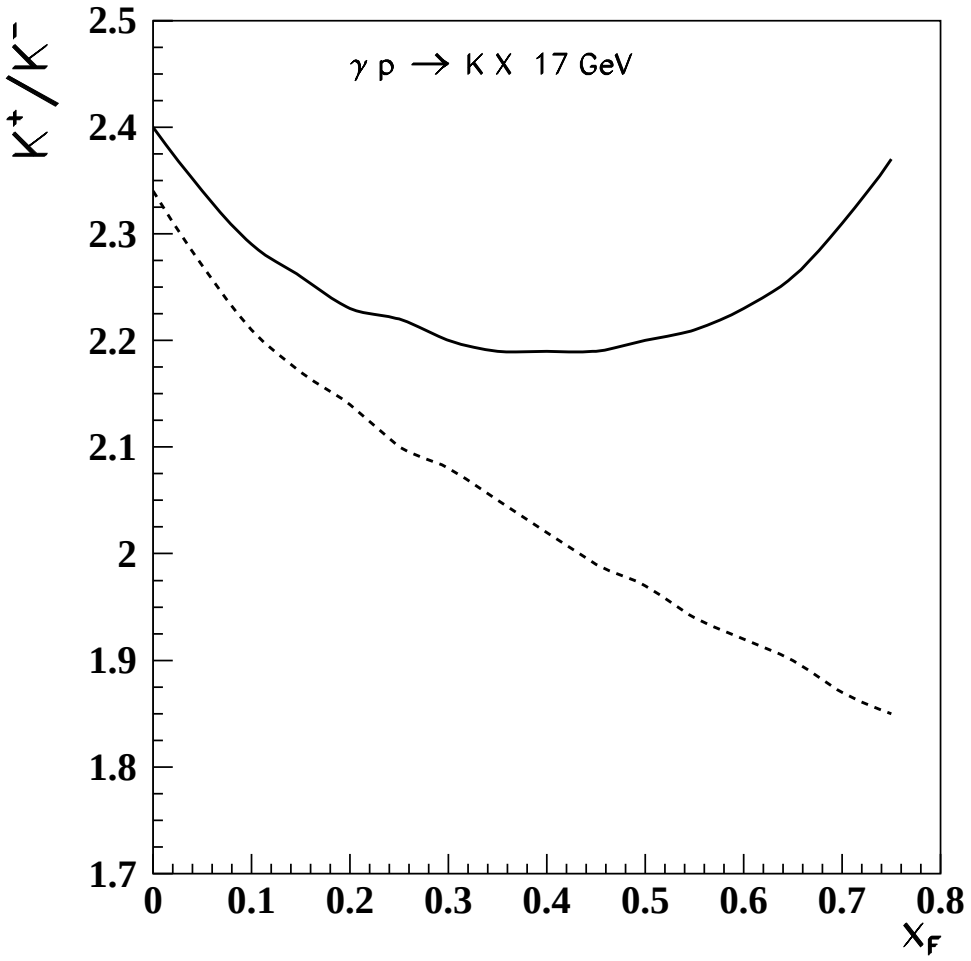

Figure 8: The QGSM prediction for the x_F dependence of the ratio of yields of charged K-mesons photoproduction at E_γ= 17 GeV.

References

[1] A. Capella, U. Sukhatme, C.I. Tan, and J. Tran Thanh Van, Phys. Rep. **236**, 225 (1994).

[2] A.B. Kaidalov, Phys. Atom. Nucl., **66**, (2003), 781.

[3] A.B. Kaidalov and K.A. Ter-Martirosyan, Yad. Fiz. **39**, 1545 (1984); Yad. Fiz. **40**, 211 (1984).

[4] G.H. Arakelyan, A. Capella, A.B. Kaidalov, and Yu.M. Shabelski, Eur. Phys. J. **C26**, 81 (2002).

[5] A.B. Kaidalov, O.I. Piskunova, Yad. Fiz. **41**, 1278 (1985).

[6] Yu.M. Shabelski, Yad. Fiz. **44**, 186 (1986).

[7] P.E. Volkovitski, Yad. Fiz. **44**, 729 (1989).

[8] A.B. Kaidalov *et al.*, Yad. Fiz. **49**, 781 (1989); Yad. Fiz. **40**, 211 (1984).

[9] N.S. Amelin *et al.*, Yad. Fiz. **51**, 941 (1990); Yad. Fiz. **40**, 211 (1984).

[10] V.V. Luigovoi, S.Yu. Sivoklokov, Yu.M. Shabelskii. Phys. Atom. Nucl. **58**, 67 (1995); Yad. Fiz. **58** (1995) 72.

[11] G.G. Arakelyan and Sh.S. Eremian, Phys. Atom. Nucl. **58**, 1241 (1995); Yad. Fiz. **58**, 132 (1995).

[12] B. Badelek and J. Kwiecinski, Rev. Mod. Phys. **68** 445 (1996).

[13] R.J. Apsimon *et al.*, Z. Phys. **C52**, 397 (1991).

[14] K. Abe *et al.*, Phys. Rev. **D32**, 2869 (1985).

[15] T.H. Bauer *et al.*, Rev. Mod. Phys. **50**, 261 (1978).

[16] G.H. Arakelyan, C. Merino, C. Pajares, and Yu.M. Shabelski, Eur. Phys. J. **C54**, 577 (2008); arXiv:0805.2248 [hep-ph].

[17] Particle Data Group, Chin. Phys. **C38**, 090001 (2014).

[18] V.A. Abramovski, V.N. Gribov, and O.V. Kancheli, Yad. Fiz. **18**, 595 (1973).

[19] A.B. Kaidalov. Yad. Fiz. **45**, 1432 (1987).

[20] J. Gandsman *et al.*, Phys. Rev. **D10**, (1974) 1562.